When bubbles matter: hydrogen transport governs apparent kinetics in 4-nitrophenol hydrogenation reaction

Tatiana Nizkaia, Philipp Groppe, Valentin Müller, Jens Harting, Susanne Wintzheimer, 4 and Paolo Malgaretti Valentin Müller, 4 and Paolo Malgaretti Valentin Mülle

¹Helmholtz-Institute Erlangen-Nürnberg for Renewable Energy (IET-2), Forschungszentrum Jülich, Cauerstraße 1, 91058 Erlangen, Germany ²Department of Chemistry and Pharmacy, Friedrich-Alexander-Universität Erlangen-Nuürnberg (FAU), Egerlandstraße 1, 91058 Erlangen, Germany ³Department of Chemistry and Pharmacy, Friedrich-Alexander-Universität Erlangen-Nürnberg (FAU), Egerlandstraße 1, 91058 Erlangen, Germany ⁴Fraunhofer-Institute for Silicate Research ISC, Neunerplatz 2, 97082 Würzburg, Germany

The reduction of 4-nitrophenol (4-NiP) with sodium borohydride is widely used to benchmark heterogeneous catalysts, yet its kinetics are commonly oversimplified as pseudo-first-order. In reality, borohydride hydrolysis and hydrogenation by dissolved hydrogen proceed concurrently, making hydrogen transport a decisive factor in shaping apparent activity. Re-examining data on $Pt-SiO_2$ supraparticles with different pore structures, we attribute contrasting kinetic behavior to distinct regimes of hydrogen transport: diffusive transport sustains pseudo-first-order kinetics, while bubble-mediated escape causes hydrogen loss and incomplete conversion. We propose a kinetic model that captures this transition and enables consistent interpretation of experimental data. More broadly, our analysis shows that apparent differences in activity during 4-NiP benchmarking can arise from hydrogen transport rather than intrinsic properties of the catalyst, underscoring the need to account for transport effects when comparing catalyst performance.

The hydrogenation of 4-Nitrophenol (4-NiP) using sodium borohydride (NaBH₄) in aqueous solutions is widely recognized as a benchmark reaction for evaluating the efficiency of heterogeneous catalysts [1–4]. This reaction is popular due to its operational simplicity and the convenience of *in situ* monitoring using UV-visible spectroscopy. Traditionally, the reaction kinetics have been described as pseudo-first-order, characterized by a single reaction rate constant which depends on initial concentrations of 4-NiP and NaBH₄ [5–7].

However, recent studies have shown that this reaction is more complex than previously thought. In fact, the catalysts used for the reaction also promote the hydrolysis of borohydride, leading to the formation of molecular hydrogen [8–10]. Since this process is much faster than the hydrogenation of 4-NiP, experiments are typically carried out with a large excess of NaBH₄ to ensure complete conversion of 4-NiP and to maintain pseudo-firstorder kinetics [1]. Also, some metals can catalyse direct hydrogenation of 4-NiP by dissolved hydrogen [9, 11, 12]. In this case, some of the hydrogen produced by hydrolysis can be used for direct 4-NiP hydrogenation [9], while the rest is transported away from the catalytic region in the form of bubbles or via diffusion, and eventually leaves the reactor. The hydrogenation rate in this case depends on the balance between hydrogen production and the rate at which it leaves the system, which ultimately depends on the onset of bubbling [13, 14]. Accordingly, as it has recently been discussed for other catalytic systems [15], transport of hydrogen becomes a crucial factor in determining the catalyst efficiency.

While deviations of 4-NiP hydrogenation kinetics from classical models have been observed previously [16–18]

(a) Hydrogenation mechanisms

(I)
$$4 \underbrace{\bigcirc_{OH}^{NO_2}}_{OH} + 3NaBH_4 \xrightarrow{Pt} 4 \underbrace{\bigcirc_{OH}^{NH_2}}_{OH} + 3NaBO_2 + 2H_2O$$

(b) Hydrogen transport

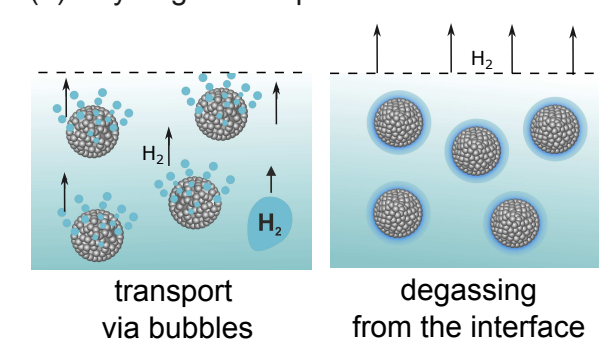


FIG. 1: (a) Reaction scheme of 4-NiP hydrogenation, depicting different mechanisms: (I) transfer hydrogenation by borohydride and (II) hydrolysis of borohydride and hydrogenation by dissolved hydrogen. (b) Sketch of hydrogen transport mechanisms: bubbling vs. degassing from the liquid/gas interface.

and a secondary hydrogenation pathway via dissolved H₂ has been acknowledged [9], the transport of hydrogen has

never been considered as a factor that can affect the reaction kinetics. In this study, we address its relevance by re-examining experimental data on the hydrogenation of 4-NiP using Pt – SiO₂ catalytic supraparticles (SPs) fabricated via spray-drying techniques [19, 20]. These SPs offer tunable porosity at a fixed catalyst loading, enabling investigations into how pore size and distribution of the catalyst affect the reaction kinetics. While assessing the catalytic activity of the obtained supraparticles using 4-NiP hydrogenation as a test reaction, we observed puzzling deviations from the expected reaction kinetics, particularly in samples that exhibit bubble formation. To address these deviations, we develop a kinetic model that includes 4-NiP hydrogenation via both transfer hydrogenation and direct hydrogenation via H₂, and takes into account the transport of hydrogen. The model reveals two distinct regimes: initially, when borohydride is plentiful, transfer hydrogenation dominates; at later stages, once borohydride is depleted, hydrogenation proceeds mostly via dissolved H₂. We use our model to analyze experimental data and find evidence for H₂-mediated hydrogenation at long times and for the influence of hydrogen transport on the apparent reaction kinetics.

Kinetic model of the two mechanisms of hydrogenation

The classical scheme of 4-NiP hydrogenation [5, 16, 21] describes a binary reaction at the surface of a catalytic metal nanoparticle as

$$4\text{-NiP} + 3\text{BH}_4^- \xrightarrow{\text{catalyst}} 4\text{-AmP} + 3\text{BO}_2^- + 2\text{H}_2\text{O}. \quad (1)$$

This process is accompanied by catalytic hydrolysis of borohydride [8],

$$BH_4^- + 4H_2O \xrightarrow{catalyst} B(OH)_4^- + 4H_2, \qquad (2)$$

which is typically much faster; hence, an excess of borohydride is required for efficient 4-NiP hydrogenation [3]. Meanwhile, some metals (in particular Pt and Pd) also catalyse a direct hydrogenation reaction which uses H₂ produced by hydrolysis [9, 11, 12]:

$$4\text{-NiP} + 3\,\mathrm{H}_2 \xrightarrow{\mathrm{catalyst}} 4\text{-AmP} + 2\,\mathrm{H}_2\mathrm{O}, \tag{3}$$

Experimental characterization of this pathway under high H₂ pressure shows a pH independence and pseudozeroth-order kinetics with respect to 4-NiP, unless 4-NiP concentrations are very small (see [11] and the Supplementary material in [9]).

Therefore, two mechanisms can coexist: transfer hydrogenation via borohydride (Eq. 1) and a two-step route via hydrolysis and H₂-mediated hydrogenation (Eqs. 2-3). When H₂ is produced, it can either leave the system or be used for 4-NiP hydrogenation. The fraction used

is controlled by the competition between hydrogenation rates and H₂ removal. Accordingly, fast transport reduces the local H₂ concentration and thus the overall conversion rate of 4-NiP. Prior to borohydride depletion, both mechanisms may be operational, leading to complex kinetics. To capture both hydrogenation pathways together with the transport of hydrogen, we use a simplified kinetic model:

$$\frac{dC_{4-\text{NiP}}}{dt} = -k_A C_{\text{H}_2} - 4k_{AB} C_{4-\text{NiP}} C_{\text{NaBH}_4}, \tag{4a}$$

$$\frac{dC_{4-\text{NiP}}}{dt} = -k_A C_{\text{H}_2} - 4k_{AB} C_{4-\text{NiP}} C_{\text{NaBH}_4},$$
(4a)
$$\frac{dC_{\text{NaBH}_4}}{dt} = -k_B C_{\text{NaBH}_4} - 3k_{AB} C_{4-\text{NiP}} C_{\text{NaBH}_4},$$
(4b)
$$\frac{dC_{\text{H}_2}}{dt} = 4k_B C_{\text{NaBH}_4} - 3k_A C_{\text{H}_2} - \alpha C_{\text{H}_2}.$$
(4c)

$$\frac{dC_{\rm H_2}}{dt} = 4k_B C_{\rm NaBH_4} - 3k_A C_{\rm H_2} - \alpha C_{\rm H_2}.$$
 (4c)

Here, C_{NaBH_4} , $C_{\text{4-NiP}}$, C_{H_2} are concentrations of the respective species, k_{AB} and k_A are effective rate constants of transfer hydrogenation and H₂-mediated hydrogenation, k_B is the hydrolysis rate, and α is the H₂ transport rate. The coefficients are effective, depending on catalyst loading, distribution, and adsorption.

Incorporating a transport term, $\alpha C_{\rm H_2}$, into the kinetic model allows us to account for the rate at which hydrogen escapes from the solution. Notably, when hydrogen is released in the form of bubbles, its evacuation rate is significantly higher than in the absence of bubbling, where hydrogen loss is limited to diffusion and evaporation from the reactor. To capture changes in the transport mechanism over the course of the reaction, we introduce a simplified, piece-wise constant model for the transport coefficient:

$$\alpha(t) = \begin{cases} \alpha_s & t < t_{bub} \\ \alpha_l & t \ge t_{bub}, \end{cases}$$
 (5)

where α_s corresponds to bubble-mediated transport, α_l to diffusive transport, and t_{bub} is the time at which bubbling stops.

Analysis of experimental data

We revisit the results of 4-NiP hydrogenation experiments described in [19] and complement them with new measurements. Composite supraparticles were obtained by spray-drying a dispersion of Pt nanoparticles and passive SiO₂ nanoparticles of different sizes with the addition of CaCl₂ salt, enabling pore-structure tuning at fixed catalyst loading (Type A and B) [19] and by spray-drying a dispersion of passive SiO₂ nanoparticles with Pt incorporated using the ALD method [20].

Type A: 182 nm $SiO_2 + 4$ nm Pt + CaCl₂. Large pores (all > 40 nm), agglomerates of Pt nanoparticles inside the supraparticles and on the surface; strong bubbling in the first 5–8 min. Dataset from [19].

Type B: 19 nm $SiO_2 + 4$ nm Pt + $CaCl_2$. Tunable pore size distribution (8–19 nm) with all pores < 40 nm;

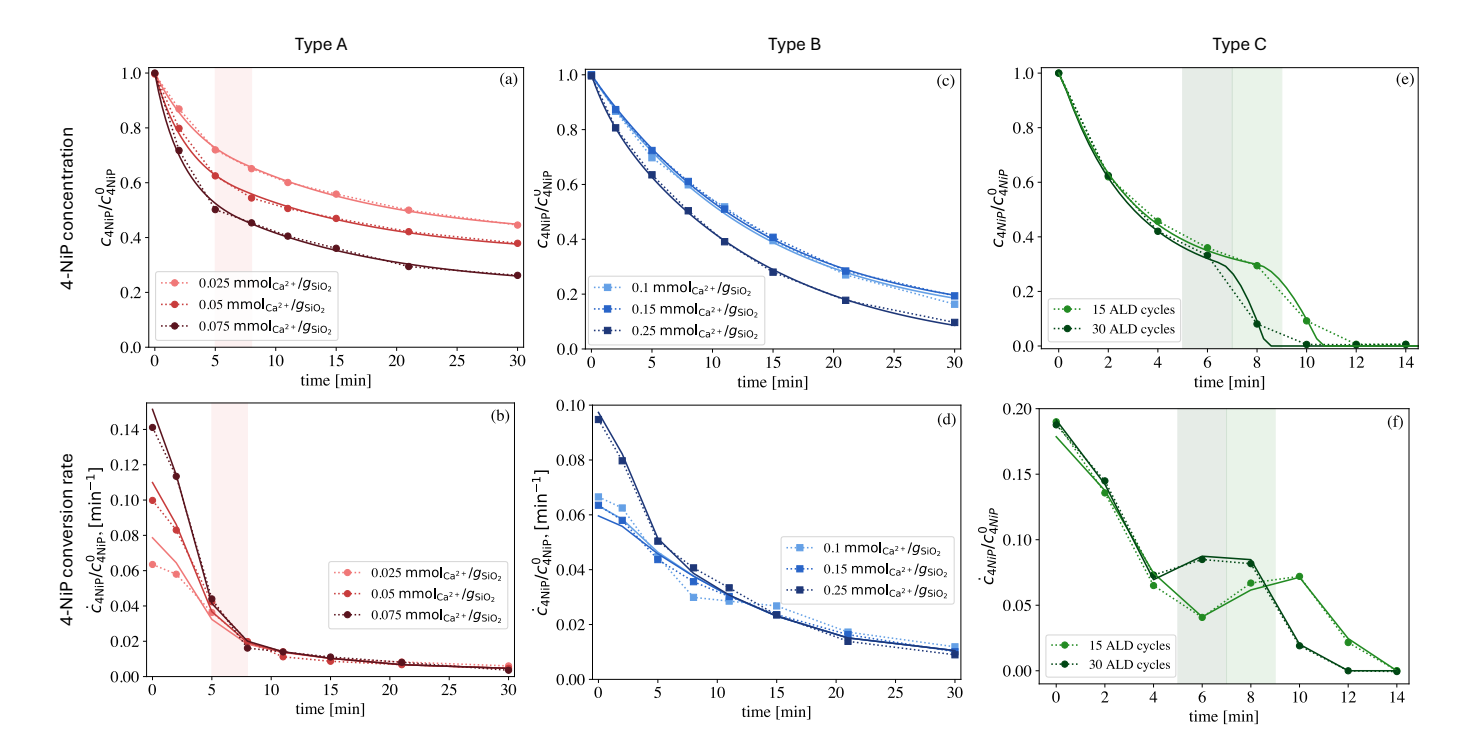


FIG. 2: Time evolution of normalized 4-NiP concentration and reaction rate for Types A (a,b), B (c,d), and C (e,f). Dotted curves with symbols: experiments; solid curves: model fits to Eqs. (4a–4c). Shaded areas: time range within which bubbling stops.

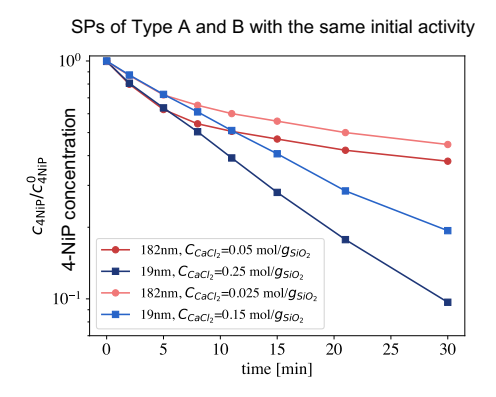


FIG. 3: Semi-logarithmic plot of normalized 4-NiP concentration for Type A and Type B supraparticles with the same initial activity.

aggregates of Pt particles inside the supraparticles; no bubbling observed. Dataset from [19].

Type C: 8 nm SiO_2 with Pt by ALD [20]. Very small pores (4 nm); small clusters of Pt atoms in a thin layer near the surface of the supraparticle. 4-NiP hydrogenation experiments performed for supraparticles with 15 and 30 ALD cycles show active bubble formation in the initial stage of the reaction: 5–7 min (30 cycles) and 7–9 min (15 cycles).

The evolution of the 4-NiP concentration for supra-

particles of Types A, B, and C is shown in Fig. 2a,c,e (experimental data are shown as symbols connected by dotted lines). While the initial hydrogenation rates for Types A and B are similar, Type A shows weaker activity at longer times and lower 4-NiP conversion after 30 min. Type C shows higher initial reaction rates compared to particles of Type A and B, and experiences an unexpected surge of activity a few minutes into the reaction.

We start by comparing the activity of Type A and Type B supraparticles, which all have the same Pt loading. Interestingly, some pairs of Type A/Type B supraparticles exhibit identical catalytic activity during the first 5 min of the reaction, but diverge markedly at longer times. As shown in Fig. 3, the concentration profiles of Type B supraparticles remain linear on a semilogarithmic scale, consistent with pseudo-first-order kinetics, whereas Type A profiles deviate after 5-8 min, indicating a transition to a different kinetic regime. To pinpoint this transition, we track the time evolution of the 4-NiP hydrogenation rate by finite-difference differentiation of the measured concentration (Fig. 2b). At short times (t < 5 min), hydrogenation rates differ between Type A samples, but at longer times (t > 5 min), the rate curves collapse. Notably, while the 4-NiP concentration at t=5min varies significantly (Fig. 2a), the rates at and beyond this point are nearly identical (Fig. 2b). This behavior is consistent with the pseudo-zeroth-order kinetics with re-

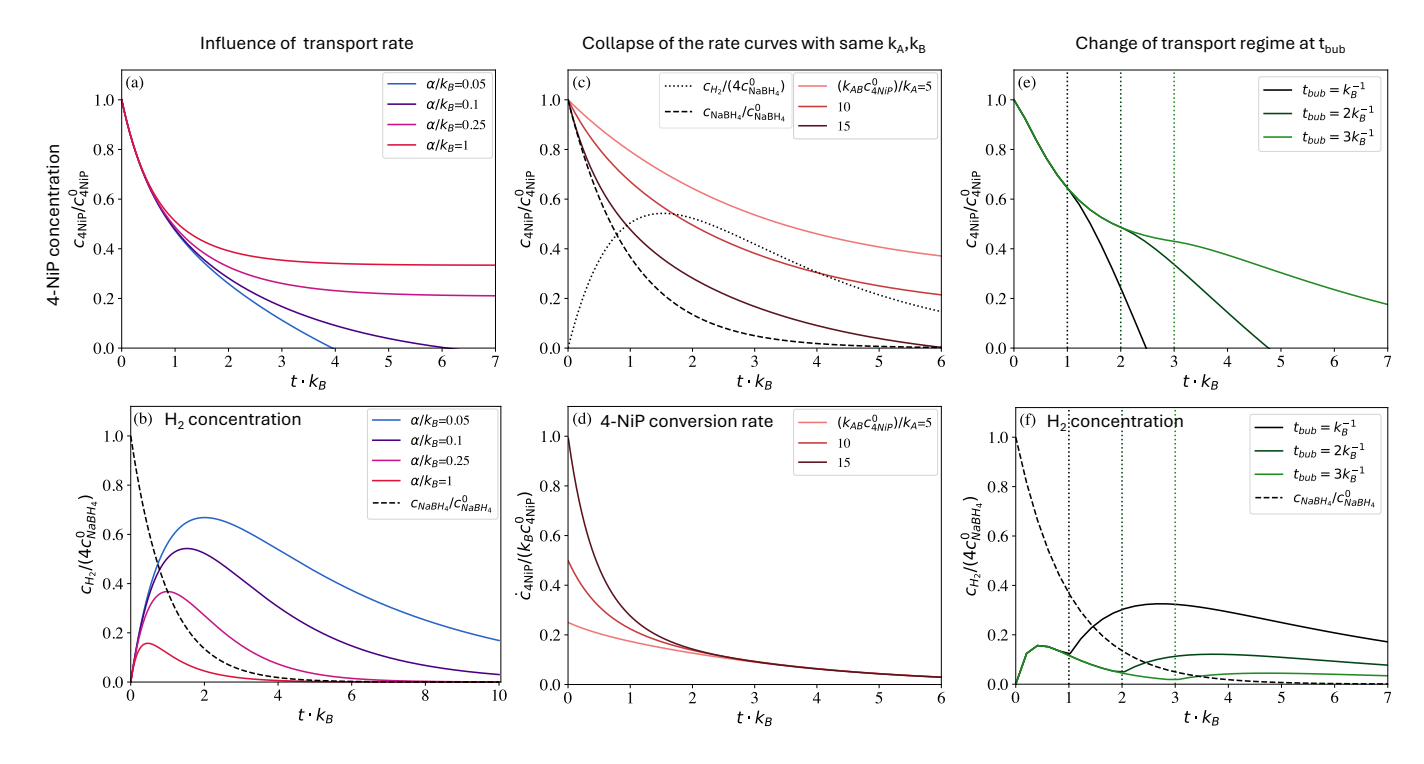


FIG. 4: Influence of the hydrogen transport coefficient on apparent kinetics: time evolution of 4-NiP (a), borohydride (b, dashed), and hydrogen (d, solid) for systems with identical k_{AB} , k_{B} , k_{A} and varying α .

spect to 4-NiP, characteristic of H_2 -mediated hydrogenation reported in Refs. [9, 11]. This can happen if most of borohydride is hydrolysed in the first few minutes of the reaction, after which H_2 -mediated hydrogenation dominates. This suggestion is consistent with the fact that production of H_2 bubbles was observed only in the first 5–8 min of the reaction [19].

To analyze the data, we use a simple kinetic model Eqs. (4a–4c), which describes two pathways of 4-NiP hydrogenation and takes into account hydrogen transport (see Supplementary material for details). Before fitting the model to experimental data, we use it to rationalize the observed kinetic features on a qualitative level.

First, our model predicts that systems with identical reaction rates $(k_{AB}, k_A, k_B, \text{ see Fig.1 and Eqs.}(4\text{a-4c}))$ and different transport rates α collapse at short times, then diverge at long times to reach different conversion levels (Fig. 4a,b). Indeed, at short times, the transfer hydrogenation dominates and the hydrogenation rate is governed by NaBH₄ concentration (dashed curve in Fig. 4a,b), which is the same for all the systems; at long times, hydrogenation proceeds via dissolved H₂, whose concentration depends on the transport rate. This is exactly what we observe for supraparticles of Types A and B with matched initial rates (see Fig. 3). We suggest that these supraparticles show, in fact, very similar catalytic activity, and the difference in their eventual efficiency is due to different mechanisms of hydrogen transport (bubbling vs. non-bubbling).

Second, our model predicts that catalytic systems can behave differently in the initial stages of the reaction but exhibit the same catalytic activity at long times (collapsing curves in Fig. 2b), if they have the same values of k_A , k_B and α but different values of k_{AB} (Fig. 4c,d). Indeed, in the initial stage, the reaction proceeds mostly via transfer hydrogenation by NaBH₄, captured by k_{AB} . However, at later times H₂-mediated hydrogenation becomes dominant. The hydrogenation rate in this region depends only on k_A and the hydrogen concentration $c_{\rm H_2}$, which, in turn, is defined by the rates of hydrolysis k_B and transport α . The collapse, depicted in Fig. 2b, suggests that supraparticles of Type A have the same catalytic activity with respect to H₂-mediated hydrogenation and hydrolysis, but different catalytic activities with respect to transfer hydrogenation.

Finally, the activity surge for Type C is captured by the time-dependent transport $\alpha(t)$ (Eq. 5), with $\alpha_s \gg \alpha_l$. This is demonstrated in Fig. 4e. When bubbling stops before NaBH₄ depletion, H₂ produced by hydrolysis accumulates in the solution (see Fig. 4f) and leads to the acceleration of H₂-mediated hydrogenation.

Given these observations, we can fit all the data with Eqs. (4a–4c,5) using minimal subsets of fitting parameters, guided by the kinetic features described above. For Type A supraparticles, all the curves in Fig. 2a are fitted with the same values for k_A , k_B , α_s , α_l and by solely varying k_{AB} (see Fig. S1 in the Supplementary Material). Indeed, the collapse of the reaction rate curves at

long times (Fig.2a) suggests that k_A (H₂-mediated hydrogenation rate) and α_l (H₂ transport rate in non-bubbling regime) are the same for all curves, and the fact that all curves collapse onto a master curve after the same characteristic time suggests that k_B (hydrolysis rate) and α_s (H₂ transport rate in bubbling regime) are the same as well. While other sets of parameters (with different values of k_A , k_B , α_s , α_l for each curve) can also reproduce the data, the observed collapse is unlikely to be coincidental, making a shared set of parameters the most natural explanation. Interestingly, it is possible to fit the data for supraparticles of Type B (non-bubbling), using the same set of shared parameters $(k_A, k_B \text{ and } \alpha_l)$ as for Type A supraparticles; however, these fits are not unique because no clear regime change is observed, making multiple mechanisms compatible with the data (see Fig. S2) in the Supplementary Material). For Type C supraparticles, the collapse of the reaction curves in the initial stage (Fig. 2e) suggests similar activity with respect to 4-NiP hydrogenation, while different bubbling times suggest different rates of borohydride hydrolysis. Accordingly, it is possible to fit these curves with the same k_{AB} , k_A , α_s , α_l but different k_B and t_{bub} . The fits are provided as solid curves in (Fig. 2a-f), with the right panels showing finite-difference derivatives of the fits on the experimental time grid. We can see that all the fits are in excellent agreement with the data.

CONCLUSION

By revisiting experimental data on Pt-SiO₂ supraparticles with different pore architectures (Types A, B, and C), we suggest that hydrogenation of 4-NiP with NaBH₄ is not governed by a single apparent rate constant but by the interplay of multiple reaction mechanisms and hydrogen transport. At early times, transfer hydrogenation via NaBH₄ dominates, while at later times, hydrogenation by dissolved H₂ becomes increasingly relevant once NaBH₄ is depleted. Which pathway prevails is determined largely by how fast H₂ is transported out of the system. Note that kinetic behavior with different apparent reaction rates at short and long times has been observed previously [16, 17], but was attributed to formation of the reaction intermediate 4-hydroxylaminophenol. However, its presence could not be readily detected and the model proposed in [16, 17] was able to describe only the initial 30% of the concentration curves. Our model provides an simple alternative explanation to this behavior: a shift from direct reaction with borohydride to hydrogenation via dissolved H_2 .

The kinetic features demonstrated by supraparticles of Type A,B,C illustrate the combined effect of two hydrogenation mechanisms and hydrogen transport: bubbling accelerates H₂ loss and leads to incomplete conversion (Fig. 2a, Fig. 4a), non-bubbling systems sustain

pseudo-first-order kinetics and achieve higher conversion (Fig. 2c, Fig. 4c), and in some cases catalytic activity surges once bubbling ceases and dissolved $\rm H_2$ accumulates (Fig. 2e,f and Fig. 4e,f). A minimal kinetic model combining the two hydrogenation pathways with time-dependent $\rm H_2$ transport reproduces these observations.

This has important implications for using 4-NiP hydrogenation as a benchmark reaction. First, catalyst performance can only be compared across studies if the hydrogen-transport mechanism is the same; bubbling and non-bubbling systems should not be directly compared. In fact, our analysis shows that supraparticles with essentially identical catalytic activity (same k_A, k_B, k_{AB}) can exhibit very different long-term behavior depending on the rate of hydrogen transport (Fig. 3, Fig. 4a). Second, it is essential to track how the transport regime evolves during the reaction. If bubbling stops before NaBH₄ is fully depleted, the concentration of dissolved H₂ rises and triggers a sudden increase in activity (Fig. 2e, Fig. 4e). Finally, 4-NiP hydrogenation is not a single reaction but a combination of transfer hydrogenation, hydrolysis, and H₂-mediated hydrogenation. Catalytic systems may therefore show different activities for each step. This is evident for Type A supraparticles with the same Pt loading but different aggregate sizes: they exhibit the same activity for H₂-induced hydrogenation (see Fig. 2b, long times) but different activities for transfer hydrogenation (see Fig.2b, short times). Concurrent measurement of H₂ production during test reactions would help disentangle these contributions and provide a more accurate assessment of catalytic performance.

Beyond 4-NiP, our analysis has a broader impact: in generic hydrogenation reactions driven by hydrogen donors, the apparent kinetics can be strongly influenced by hydrogen transport. For example, a dual hydrogenation mechanism similar to the one we described has been reported for formic acid and related donors, where both direct hydride transfer and H₂ production take place [22– 26]. This suggests that the transport effects identified here are not confined to a model system, but are representative of a wider class of transfer hydrogenation reactions. Mechanistic analysis of catalytic performance should therefore account for the transport and fate of in situ generated H₂, since it can alter observed kinetics even when the underlying chemistry remains unchanged. Finally, transport effects are expected to play an important role in continuous-flow reactors [27–30].

ACKNOWLEDGMENTS

We acknowledge funding by the Deutsche Forschungsgemeinschaft (DFG, German Research Foundation)—Project No. 431791331—SFB 1452.

- P. Herves, M. Pérez-Lorenzo, L. M. Liz-Marzán, J. Dzubiella, Y. Lu, and M. Ballauff, Chemical Society Reviews 41, 5577 (2012).
- [2] M. Goepel, M. Al-Naji, P. With, G. Wagner, O. Oeckler, D. Enke, and R. Gläser, Chemical Engineering & Technology 37, 551 (2014).
- [3] T. Aditya, A. Pal, and T. Pal, Chemical Communications 51, 9410 (2015).
- [4] T. K. Das and N. C. Das, International Nano Letters 12, 223 (2022).
- [5] S. Wunder, F. Polzer, Y. Lu, Y. Mei, and M. Ballauff, The Journal of Physical Chemistry C 114, 8814 (2010).
- [6] S. R. Thawarkar, B. Thombare, B. S. Munde, and N. D. Khupse, RSC advances 8, 38384 (2018).
- [7] A. Iben Ayad, D. Luart, A. Ould Dris, and E. Guénin, Nanomaterials 10, 1169 (2020).
- [8] S. Varshney, D. Meyerstein, R. Bar-Ziv, and T. Zidki, Molecules 28, 6530 (2023).
- [9] R. Grzeschik, D. Schäfer, T. Holtum, S. Küpper, A. Hoff-mann, and S. Schlücker, The Journal of Physical Chemistry C 124, 2939 (2020).
- [10] A. Serrà, R. Artal, M. Pozo, J. Garcia-Amorós, and E. Gómez, Catalysts 10, 458 (2020).
- [11] M. J. Vaidya, S. M. Kulkarni, and R. V. Chaudhari, Organic Process Research & Development 7, 202 (2003).
- [12] C. Paun, G. Słowik, E. Lewin, and J. Sá, RSC Advances 6, 87564 (2016).
- [13] A. Oehmichen, L. Datsevich, and A. Jess, Chemical Engineering & Technology 33, 883 (2010).
- [14] T. Solymosi, M. Geißelbrecht, S. Mayer, M. Auer, P. Leicht, M. Terlinden, P. Malgaretti, A. Bösmann, P. Preuster, J. Harting, et al., Science advances 8, eade3262 (2022).
- [15] H. H. Heenen et al., Nature Catalysis 7, 106 (2024).

- [16] S. Gu, S. Wunder, Y. Lu, M. Ballauff, R. Fenger, K. Rademann, B. Jaquet, and A. Zaccone, The Journal of Physical Chemistry C 118, 18618 (2014).
- [17] S. Gu, Y. Lu, J. Kaiser, M. Albrecht, and M. Ballauff, Physical Chemistry Chemical Physics 17, 28137 (2015).
- [18] M. Li and G. Chen, Nanoscale 5, 11919 (2013).
- [19] P. Groppe, J. Reichstein, S. Carl, C. Cuadrado Collados, B.-J. Niebuur, K. Zhang, B. Apeleo Zubiri, J. Libuda, T. Kraus, T. Retzer, et al., Small p. 2310813 (2024).
- [20] P. Groppe, V. Müller, J. Will, X. Zhou, K. Zhang, M. S. Moritz, C. Papp, J. Libuda, T. Retzer, E. Spiecker, et al., Chemistry of Materials 37, 2815 (2025).
- [21] S. Saha, A. Pal, S. Kundu, S. Basu, and T. Pal, Langmuir 26, 2885 (2010).
- [22] D. A. Berry, A. Smith, M. E. Jones, and D. G. Blackmond, Faraday Discussions 220, 45 (2019).
- [23] R. Nie, X. Jin, X. Chen, and G. Lu, ACS Catalysis 11, 524 (2021).
- [24] Y. Zhang, W. Li, F. Li, J. Li, W. Xue, M. Zhao, and Y. Wang, New Journal of Chemistry 48, 664 (2024).
- [25] Z. Yu and J. Spencer, Chemical Communications pp. 1993–1994 (1998).
- [26] R. Javaid, T. Yamaguchi, A. Tanimu, A. Fayyaz, T. Kimura, and N. Itoh, Beilstein Journal of Organic Chemistry 9, 2109 (2013).
- [27] A. Iben Ayad, E. Guénin, and A. Ould Dris, Journal of Flow Chemistry 12, 101 (2022).
- [28] J. Park, J. S. Maier, C. Evans, M. Hatzell, S. France, C. Sievers, and A. S. Bommarius, ACS Sustainable Chemistry & Engineering 13, 5906 (2025).
- [29] V. Lomonosov, A. Popova, O. Gubanova, V. Nevedomskiy, A. Garshev, S. Cherepanova, P. Gushchin, A. Nechaev, and S. Varfolomeev, Reaction Chemistry & Engineering 7, 1109 (2022).
- [30] M. Ali, S. Kumar, R. Patel, N. Verma, and A. Singh, ACS Omega 9, 12345 (2024).

Supplementary materials

KINETIC MODEL WITH HYDROGEN TRANSPORT

To capture both hydrogenation pathways we use a simplified kinetics model:

$$\frac{dC_{4-\text{NiP}}}{dt} = -k_A C_{\text{H}_2} - 4k_{AB} C_{4-\text{NiP}} C_{\text{NaBH}_4}, \tag{1a}$$

$$\frac{dC_{4\text{-NiP}}}{dt} = -k_A C_{\text{H}_2} - 4k_{AB} C_{4\text{-NiP}} C_{\text{NaBH}_4}, \qquad (1a)$$

$$\frac{dC_{\text{NaBH}_4}}{dt} = -k_B C_{\text{NaBH}_4} - 3k_{AB} C_{4\text{-NiP}} C_{\text{NaBH}_4}, \qquad (1b)$$

$$\frac{dC_{\rm H_2}}{dt} = 4k_B C_{\rm NaBH_4} - 3k_A C_{\rm H_2} - \alpha C_{\rm H_2}.$$
 (1c)

where k_{AB} , k_A are the effective rate constants of transfer hydrogenation via borohydride and via dissolved hydrogen, k_B is the effective rate constant of hydrolysis of borohydride and α is the rate at which hydrogen leaves the solution.

In order to minimize the number of parameters, we use the following simplifications in deriving the model.

First, we use an effective pseudo zeroth-order reaction scheme for H_2 mediated hydrogenation of 4-NiP at all times. The effective pseudo zeroth order kinetics observed in the experiments [1, 2] supposedly follows from the microscopic binding-unbinding kinetics of 4-NiP to the Pt nanoparticles and the reaction of the adsorbed species with dissolved hydrogen (Eley-Rideal mechanism [3]):

$$\frac{dC_{4\text{-NiP}}}{dt} = k_A \theta_{4\text{-NiP}} C_{H_2},\tag{2}$$

where k_A is proportional to the available surface of the catalyst and $\theta_{4\text{-NiP}}$ is the fraction of the catalyst occupied with 4-NiP:

$$\theta_{\text{4-NiP}} = \frac{K_{\text{4-NiP}}}{1 + K_{\text{4-NiP}}C_{\text{4-NiP}}},$$
 (3)

where $K_{4\text{-NiP}}$ is the adsorption equilibrium constant of 4-NiP. When $K_{4\text{-NiP}}C_{4\text{-NiP}} \gg 1$, $\theta_{4\text{-NiP}} \approx 1$ and the kinetics is pseudo zero-the order in 4-NiP. This behavior is expected to break at small densities of 4-NiP, where the full equation for coverage has to be taken into account.

Second, we do not explicitly use Langmuir-Hinschelwood model [4] (accounting for the competition of the reactants for the active sites at the catalyts) to descrive the surface reaction between borohydride and 4-NiP. In the literature [5–7] Langmuir-Hinschelwood approach is used to fit the dependence of the short term apparent reaction rate k_{app} on initial concentrations. We use instead a simple binary reaction term with an effective rate coefficient k_{AB} , which can also depend on the initial concentrations of reactant.

Third, we use here a linear dependency of the hydrogen evaporation flux on concentration, assuming that the

saturation concentration of H₂ is small compared to typical concentrations in the course of the reaction, and can be neglected. This is indeed the case for evaporation from the interface in contact with the atmosphere, since H_2 is lighter than air and does not accumulate near the interface.

Finally, we have disregarded all back-reactions, since our focus is mainly on the intermediate stages of the time evolution of the 4-NiP concentration, rather than on the eventual equilibrium state or on the initial short term effects. In particular, we disregard here the induction period, associated with the back-reaction of 4-aminophenol with dissolved oxygen [8–11], because for concentrations of NaBH₄ use in the experiments it is shorter than the time resolution of our measurements.

To take into account the transition between bubbling and non-bubbling regimes for particles of Type A, we use a piece-wise constant dependency of hydrogen transport rate on time:

$$\alpha(t) = \begin{cases} \alpha_s & t < t_{bub} \\ \alpha_l & t \ge t_{bub}, \end{cases} \tag{4}$$

where α_s is the rate of hydrogen transport by bubbles, and α_l is the rate of hydrogen transport by diffusion and evaporation from the surface of the reaction mixture.

While the onset and cessation of bubbling is associated with the concentration of dissolved hydrogen, we consider here a simplified scheme, where bubbling goes on for a fixed time t_{bub} , which was taken from experimental observations.

EXPERIMENTAL SETUP AND SUPERPARTICLE CHARACTERIZATION

In all benchmarking experiments, a small amount of 4-NiP with suspended supraparticles (SPs) was mixed with an aqueous solution of sodium borohydride (NaBH₄) to match the following initial concentrations: C_{4-NiP} = $6 \cdot 10^{-5} M$, $C_{\text{NaBH}_4} = 0.1 M$ and the initial pH of the reaction mixture was set to pH ≈ 10.4 by NaOH addition. The dilution of the SP suspension (fraction of supraparticle volume related to the volume of the solvent) is $\chi = 0.03$. The time evolution of the 4-NiP concentration was monitored through UV/Vis spectroscopy and the relative concentration of 4-NiP is calculated as:

$$c_{4\text{-NiP}}(t) = \frac{C_{4\text{-NiP}}(t)}{C_{4\text{-NiP}}(0)} = \frac{A(t)}{A(0)},$$
 (5)

where A(t) is the amplitude of the absorbance peak corresponding to 4-NiP at time t [12].

Type A: Supraparticles with 182 nm $SiO_2 + 4$ nm Pt nanoparticles, varying concentrations of ${\rm CaCl_2}$ added during fabrication. Particles of this set consist of 4 nm Pt nanoparticles embedded in a matrix of 182 nm ${\rm SiO_2}$ nanoparticles. These supraparticles feature relatively large pores (all pores larger than 40 nm, see Fig.S19b and Table S4 in Ref. [12]), and Pt nanoparticles form agglomerates both inside the SP and on its surface. Changing the salt concentration during fabrication does not significantly alter the pore structure, but does affect the size and distribution of the Pt agglomerates [12] throughout the particle. The Pt loading measured via inductively coupled plasma atomic emission spectroscopy (ICP AES) is $0.9\,{\rm mg_{Pt}/g_{SiO_2}}$.

Type B: Supraparticles with 19 nm SiO_2+4 nm Pt nanoparticles and varying concentrations of CaCl_2 added during fabrication. Particles of this set consist of 4 nm Pt nanoparticles embedded in a matrix of 19 nm SiO_2 nanoparticles. Using varying salt concentration during fabrication allows to tune the pore size distribution of the supraparticles. Higher salt concentrations correspond to larger pores, shifting the average pore diameter from 8 nm to 19 nm (see Fig.7d and Table 1 in Ref. [12]). However, even for the highest salt concentration all pores are smaller than 40 nm (see Fig.7d in Ref. [12]). The Pt loading measured via ICP AES is $0.94\,\mathrm{mg}_{Pt}/\mathrm{g}_{\mathrm{SiO}_2}$ (similar to Type A particles).

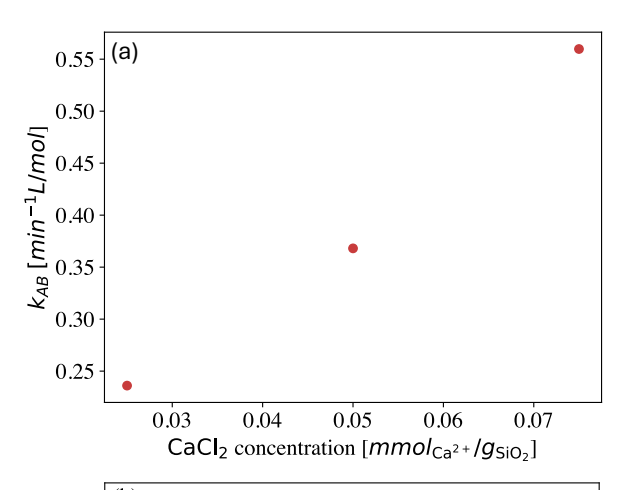
Type C: 8 nm SiO₂ with Pt by ALD [13]. Particles of this set have been fabricated using Atomic layer deposition (ALD) of Pt on spray-dried SiO₂ supraparticles. These particle feature very small (2-7 nm) pores and small clusters of Pt atoms in a thin layer near the surface. Pt loadings measured via ICP AES are $7.5\,\mathrm{mg}_{Pt}/\mathrm{g}_{\mathrm{SiO}_2}$ for 15 ALD cycles, and $14\,\mathrm{mg}_{Pt}/\mathrm{g}_{\mathrm{SiO}_2}$ for 30 ALD cycles (much higher than for Type A and B).

FITTING THE DATA

We fit the data presented in using the theoretical model governed by Eqs. (1). Not surprisingly, having 4 fitting parameters for each experimental curve allows us to fit all the experimental data with high accuracy. However, is it to be expected that upon changing the concentration of $CaCl_2$ all the rate constants have to change?

First, we can expect that the hydrogen transport rate α in the non-bubbling regime should be the same for all supraparticles, because it is associated with the rate of H_2 evaporation from the reactor. Indeed, we can extract α by fitting the experimental data for t>7 min. For both types of particles an excellent fit is obtained with $\alpha=0.075$ min⁻¹. Second, the collapse of the experimental data for t>7 min (see Fig. 4b in the main text) implies that both the hydrolysis of borohydride and the hydrogenation of 4-NiP via dissolved H_2 occur at very similar rates for the particles of this set i.e. k_A and k_B should be the same for all Type A supraparticles.

Interestingly, it is indeed possible to fit all the data for



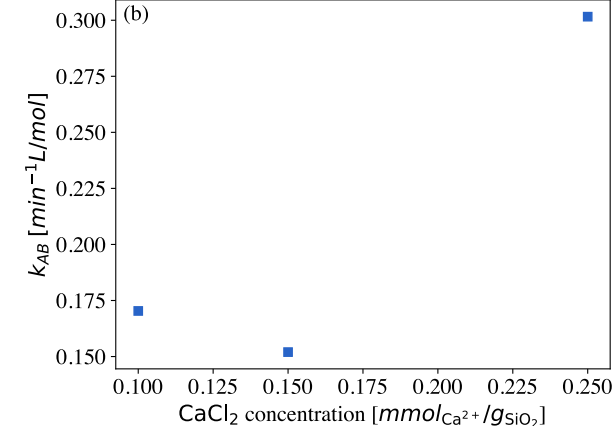


FIG. S1: Fitted values of k_{AB} for supraparticles made of 182 nm (a) and 19 nm SiO₂ supraparticles (b) versus salt concentration used during fabrication. Fitting performed using the model Eq.(1a-1c) with parameters defined by Eq.(10).

particles of Type A and Type B with the same values of $k_A, k_B, \alpha_s, \alpha_l$ and t_{bub} taken from the experiment, by solely varying k_{AB} . We use the following set of common parameters:

$$k_B = 0.45 \text{min}^{-1}, k_A = 8.75 \cdot 10^{-6} \text{ min}^{-1},$$

 $\alpha_l = 0.075 \text{ min}^{-1}, \alpha_s = 0.275 \text{ min}^{-1},$ (6)

and the following values of bubbling time, based on experimental observations:

Type A:
$$t_{bub} = 7 \min$$
, (7)

Type B (non-bubbling):
$$t_{bub} = 0 \,\text{min}.$$
 (8)

The values of k_{AB} are fitted for each curve individually, and are provided in Fig. S1. For particles of Type A hydrogenation rate constant k_{AB} increases with the amount of salt added during supraparticle fabrication. This is in line with the fact that the average size of Pt agglomerates decreases with the increase of $CaCl_2$ concentration [12], exposing a larger surface area of Pt.

SPs of Type B: fitting the data with different reaction mechanisms

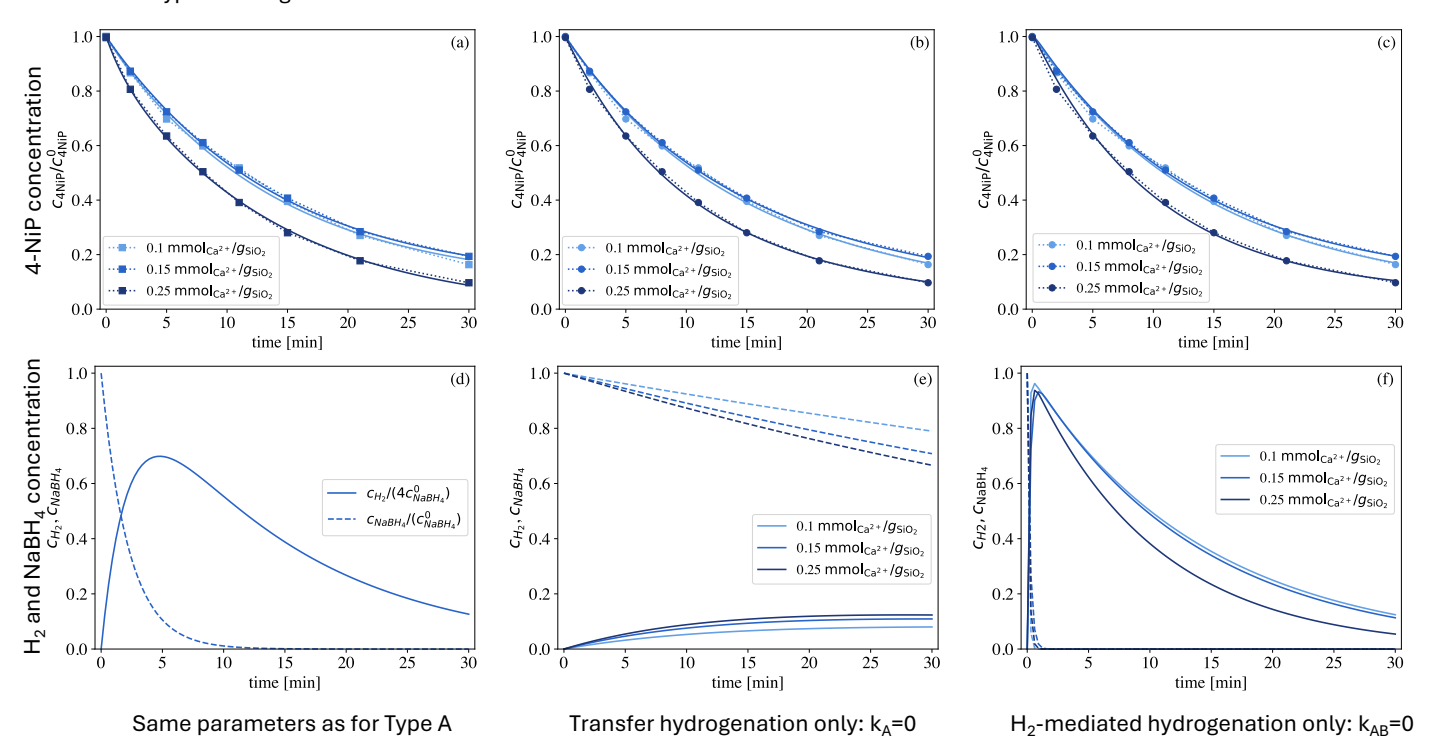


FIG. S2: 4-NiP concentration (top) and modeled H_2 concentration (bottom) for particles with 19 nm SiO₂ grains, fabricated with different concentrations of CaCl₂. Solid lines are fits using Eqs. (1) with the following sets of parameters: (a,d) k_A , k_B , α defined by Eq.(10) and varying k_{AB} (same parameters as for 182 nm) (b,e) $k_A = 0$, $\alpha = 0.075 \text{min}^{-1}$ and k_{AB} , k_B fitted for each curve (hydrogenation only by surface reaction with borohydride), (c,f) $k_{AB} = 0$ and fitted k_A , k_B , α (hydrogenation only by dissolved H_2).

However, the collapse of the experimental conversion rate curves, suggests that the amount of catalyst available to catalyze H₂-mediated hydrogenation of 4-NiP is the same for all supraparticles. Otherwise we would expect different reaction rates, k_A , for different salt concentrations. These two apparently contradicting aspects can coexist if we assume that some catalytic sites in loose agglomerates are inaccessible to co-adsorption of borohydride and 4-nitrophenolate ions because of strong electrostatic repulsion, which can be reduced by increasing the ionic strength of the solution. For supraparticles of Type B the fitted hydrogenation rate constants k_{AB} are close to those for Type A, ensuring similar conversion rates at the initial time. The only parameter responsible for the difference in long-term behavior between the two types of particles is the hydrogen transport rate in the initial stage of the reaction, α_s for Type A and α_l for Type B.

We remark, that the set of fitting parameters chosen above is not unique. Indeed, while the long-term collapse of the reaction rate curves for Type A particles imposes clear restrictions on the reaction rate coefficients, the data for supraparticles of Type B is compatible with different scenarios. As shown in the top panels of Fig. S2, the same data can be fitted successfully using different

assumptions. For example, the fit shown in Fig. S2a accounts for both chemical pathways at the same time and uses the same values k_A , k_B , α as for Type A particles and varying k_{AB} . The fit in Fig.S2b accounts only for transfer hydrogenation of 4-NiP by NaBH₄ with $k_A = 0$, the same values of k_B for all curves and varying k_{AB} . Finally, Fig. S2c shows a fit assuming only H₂-mediated hydrogenation of 4-NiP, with $k_{AB} = 0$ and varying k_A , k_B , α . Therefore, in this case it is not possible to identify the relative importance of the two chemical pathways by studying only the evolution of 4-NiP concentration. However, while the resulting $c_{4\text{-NiP}}$ curves are very similar, the time evolution of the H₂ concentration in the solution is different, as shown in the corresponding bottom panels in Fig. S2. The bottom panels of Fig. S2 show that the full model accounting for both chemical pathways leads to a time evolution of the H₂ concentration on a time scale, similar to what was observed for the H_2 flux in experiments on concurrent hydrolysis and 4-NiP hydrogenation (see Fig. 1b in [14]). At variance, accounting for solely one of the two chemical pathways leads to either monotonic growth of the concentration of H_2 (Fig.S2e)¹, or a very steep surge of H_2 concentration (Fig.S2f), followed by slow relaxation.

Therefore, our model suggests a route to identify the underlying chemical pathway by performing simple additional measurements. In fact, since in our model, Eqs. (1), the outflow of hydrogen is proportional to its concentration, measuring of H_2 flux in the experimental condition may differentiate between the different reaction mechanisms. Note, that the measurements of hydrogen flux do not need to be very precise: it is sufficient to estimate whether the flux increases, decreases or experiences a non-monotonous evolution in time.

While different sets of parameters may be used to fit the experimental curves with the model in Eqs. (1), we find the one proposed in Eq.(10) particularly interesting since it allows us to fit all experimental curves upon varying a single parameter k_{AB} . This means that the experimental data are compatible with the assumption that the morphology of the Pt-aggregates mostly affects the surface reaction between 4-NiP and borohydride ions $NaBH_4$, while H_2 -mediated hydrogenation and hydrolysis are much less affected. The latter is not so surprising: it is known that hydrolysis of borohydride happens even without a catalyst [15]. While the initial steps of this multistep reaction are slow at high pH, the subsequent steps are much faster and can proceed in the bulk [2, 16]. Also, it is widely accepted that 4-NiP has a relatively high adsorption constant to Pt [2, 5], which in particular leads to the fact that H_2 -mediated hydrogenation rate does not depend on the local 4-NiP concentration (pseudo zeroth order reaction). In absence of hydrogen sources (after depletion of borohydride), the distribution of H_2 inside the catalytic supraparticle quickly becomes uniform, so that the total hydrogenation rate (and hence the effective hydrogenation rate coefficient k_A) does not depend on the Pt distribution inside the catalytic supraparticle, but only on its total amount. In contrast, borohydride ions have a small adsorption constant due to electrostatic repulsion, making the transfer hydrogenation rate very sensitive to the local concentration of borohydride, the morphology of the aggregates and the ionic strength of the solution.

To fit the data for particles of Type C we use the following common parameters:

$$k_{AB} = 0.26 \,\mathrm{min}^{-1} \mathrm{L/mol}, k_B = 0.3 \,\mathrm{min}^{-1}$$
 (9)

$$\alpha_l = 0.075 \,\mathrm{min}^{-1}, \,\alpha_s = 7.5 \,\mathrm{min}^{-1}, \,$$
 (10)

with bubbling times estimated from experiment:

15 ALD:
$$t_{bub} = 8 \min$$
 (11)

30 ALD:
$$t_{bub} = 6 \text{min.}$$
 (12)

The fitted values of hydrogenation rate coefficients are $k_A = 6 \cdot 10^{-4} \text{min}^{-1}$ for particles fabricated with 15 ALD cycles and $k_A = 6.5 \cdot 10^{-4} \text{min}^{-1}$ for particles fabricated with 30 ALD cycles. Very similar fits can be obtained by fixing k_A and varying k_B or by varying both.

- M. J. Vaidya, S. M. Kulkarni, and R. V. Chaudhari, Organic Process Research & Development 7, 202 (2003).
- [2] R. Grzeschik, D. Schäfer, T. Holtum, S. Küpper, A. Hoff-mann, and S. Schlücker, The Journal of Physical Chemistry C 124, 2939 (2020).
- [3] D. D. Eley and E. K. Rideal, Proceedings of the Royal Society of London. Series A, Mathematical and Physical Sciences 178, 429 (1938), URL https://doi.org/ 10.1098/rspa.1938.0061.
- [4] I. Langmuir and C. N. Hinshelwood, Transactions of the Faraday Society 24, 662 (1928).
- [5] S. Wunder, F. Polzer, Y. Lu, Y. Mei, and M. Ballauff, The Journal of Physical Chemistry C 114, 8814 (2010).
- [6] S. Gu, S. Wunder, Y. Lu, M. Ballauff, R. Fenger, K. Rademann, B. Jaquet, and A. Zaccone, The Journal of Physical Chemistry C 118, 18618 (2014).
- [7] A. Iben Ayad, D. Luart, A. Ould Dris, and E. Guénin, Nanomaterials 10, 1169 (2020).
- [8] Z. Wu, J. Zhu, W. Wen, X. Zhang, and S. Wang, Journal of Solid State Chemistry 311, 123116 (2022).
- [9] E. Menumerov, R. A. Hughes, and S. Neretina, Nano letters 16, 7791 (2016).
- [10] J. Strachan, C. Barnett, A. F. Masters, and T. Maschmeyer, ACS Catalysis 10, 5516 (2020).
- [11] R. D. Neal, E. Menumerov, R. A. Hughes, and S. Neretina, The Journal of Physical Chemistry C 123, 18702 (2019).
- [12] P. Groppe, J. Reichstein, S. Carl, C. Cuadrado Collados, B.-J. Niebuur, K. Zhang, B. Apeleo Zubiri, J. Libuda, T. Kraus, T. Retzer, et al., Small p. 2310813 (2024).
- [13] P. Groppe, V. Müller, J. Will, X. Zhou, K. Zhang, M. S. Moritz, C. Papp, J. Libuda, T. Retzer, E. Spiecker, et al., Chemistry of Materials 37, 2815 (2025).
- [14] S. Varshney, D. Meyerstein, R. Bar-Ziv, and T. Zidki, Molecules 28, 6530 (2023).
- [15] R. E. Mesmer and W. L. Jolly, Inorganic Chemistry 1, 608 (1962).
- [16] F. T. Wang and W. L. Jolly, Inorganic Chemistry 11, 1933 (1972).